aerospace

MDPI

Article

Service-Aware Criticality Assessment of Inter-Satellite Links in LEO Satellite Networks

Xuyu Ni [1], Kechang Qian [2,*] and Jiayue Deng [1]

[1] Graduate School, Space Engineering University, Beijing 101416, China; isnixy@163.com (X.N.); d_jy@hgd.edu.cn (J.D.)
[2] School of Space Information, Space Engineering University, Beijing 101416, China
* Correspondence: qiankechang@126.com

Abstract

Low-Earth-Orbit (LEO) satellite networks are essential infrastructure for global broadband services. However, their time-varying topology and non-uniform ground traffic distribution hinder traditional centrality-based methods from identifying service-critical inter-satellite links. This paper proposes a Service-Aware Link Criticality (SALC) framework. An event-driven temporal graph and a gravity model capture topology dynamics and traffic distribution. Three complementary metrics are designed: weighted coverage contribution, multipath traffic allocation, and vulnerability propagation potential. These metrics assess link failures from the aspects of coverage, traffic, and delay, respectively. A CRITIC-entropy hybrid weighting method and TOPSIS produce a unified criticality ranking. Experiments on Starlink data show that SALC outperforms baseline methods. It also detects critical links missed by topology-based approaches, confirming its effectiveness.

Keywords: LEO satellite network; link criticality; service awareness; temporal graph; multi-attribute decision making

1. Introduction

In recent years, advances in reusable launch vehicles and mass-production technologies for satellites have substantially reduced the cost of deploying space assets, thereby accelerating the development of large-scale satellite constellations in LEO [1,2]. Prominent examples include Starlink, OneWeb, and Kuiper, each comprising thousands of satellites and delivering global wireless communication services [3]. Compared with geostationary Earth orbit (GEO) satellites, LEO satellites operate at much lower altitudes, which results in lower propagation losses and shorter transmission delays. Through dense constellation configurations that achieve global coverage, LEO provide space-based infrastructure for various applications, including broadband access in remote regions, aviation and maritime communications, emergency disaster response, and military communications [4].

Owing to the high-speed orbital motion of satellites, the network topology changes dynamically, and inter-satellite links (ISLs) experience intermittent connectivity [5]. Meanwhile, LEO satellites are constantly exposed to a complex space environment with strong radiation, temperature fluctuations, and solar wind disturbances. Consequently, node and link failures are highly probable, and in-orbit repairs are difficult, which challenges the continuity of end-to-end service transmission [6,7]. When a node or link fails, the impact propagates along the topology and can trigger cascading failures, leading to widespread

Check for updates

Academic Editor: Xiaofeng Wu

Received: 20 August 2026
Revised: 4 October 2026
Accepted: 14 October 2026
Published: 16 October 2026

Copyright: © 2026 by the authors. Licensee MDPI, Basel, Switzerland. This article is an open access article distributed under the terms and conditions of the Creative Commons Attribution (CC BY) license.

service disruptions [8]. Therefore, identifying high-criticality inter-satellite links and investigating their impact on end-to-end service performance are key to enhancing the resilience of constellation networks.

Identifying key nodes and links is fundamental to evaluating network resilience and vulnerability. Current approaches can be broadly divided into topology-based centrality measures and service-aware methods.

The topological centrality paradigm relies on the structural information of network graphs and uses classical metrics such as degree centrality, betweenness centrality, and eigenvector centrality to evaluate the importance of nodes or links within a network [9–11]. Given the rapid changes in LEO satellite network topology, existing studies have extended static centrality measures to dynamic time-varying scenarios, identifying critical nodes via time-aggregated graphs and graph embedding [12–14]. Beyond node-level analysis, link-level temporal centrality has also attracted increasing attention. Zhang et al. [15] proposed labeling-based centrality methods for identifying critical edges on temporal graphs, computing edge closeness and betweenness centralities. Pan and Saramäki [16] generalized path length and centrality to temporal networks. Buß et al. [17] systematically studied temporal betweenness variants applicable to both nodes and edges. In satellite networks, Zhang et al. [18] defined temporal centrality metrics using time-varying graphs to identify central nodes or links. Bi [19] proposed a "critical link sequence" to evaluate links in conjunction with topological temporal evolution, showing that delay can serve as a basis for network vulnerability assessment. Deng [20] analyzed the spatiotemporal characteristics of time-varying bottleneck links in LEO satellite networks and revealed their critical importance to network security.

These topology-driven link evaluation methods are based purely on network connectivity and do not consider the spatially non-uniform distribution of ground-based service demands. Guo [21] proposed a service-aware temporal betweenness metric that models massive satellite constellations as discrete temporal graphs to quantify the temporal criticality of nodes for specific end-to-end communication services. Gong [22] designed a multi-satellite criticality metric to quantify the multidimensional impact of satellite node set failures on regional service capacity. Liu [23] proposed the CosmoBalancer service-aware load balancing system, which ensures the reliability of critical services by periodically monitoring satellite load and network congestion. Although these methods introduce service awareness, their evaluation objects remain at the node or system level, and link-level evaluation of service performance degradation remains underexplored.

The core service of a satellite network, end-to-end data transmission, is carried by paths, and a path consists of a sequence of nodes and links. Links are the direct channels for data transmission, while nodes perform forwarding and switching. A node failure removes all incident links simultaneously, interrupting all paths that pass through the node, and its impact on service is mainly realized through the interruption of these incident links. In contrast, a link failure removes only one edge and affects only the paths that traverse that edge; the remaining traffic can still be rerouted over alternative paths. Therefore, service performance degradation is ultimately manifested at the link level, and link criticality more directly reflects service performance degradation than node criticality. Because the network performance response to topology changes is nonlinear, the joint effect of a node failure cannot be decomposed into the sum of individual link failure effects, and node criticality cannot be directly mapped to link criticality. This indicates that service-aware evaluation should treat links as the basic objects, rather than simply aggregating endpoint node scores or merely counting path traversals.

Based on the above analysis, this paper proposes the SALC framework, which directly evaluates the service performance degradation caused by a single ISL failure. It fuses three

link-level service metrics, using hybrid CRITIC-entropy weighting and TOPSIS to achieve an objective ranking. Existing service-aware methods are based on node or node-set failures. SATB is a node-level metric that measures the participation of a node in paths rather than the service performance degradation caused by a single link failure. It cannot distinguish the individual contributions of incident links, and a high node score does not imply that every incident link is critical. Gong et al. and Liu et al. study the impact of node-set failures on regional service capacity and system-level load balancing, respectively, both focusing on aggregate impacts at the node or system level. Unlike these methods, SALC directly evaluates links, avoiding the service-contribution ambiguity caused by node-level aggregation. It identifies service-critical links that topology-based methods may miss, providing a basis for link-level protection and rerouting.

The main contributions are as follows:

(1) While existing research on satellite network resilience has primarily focused on analyzing topological critical elements and evaluating service-aware nodes, this paper concentrates on the criticality of ISL to services.
(2) A service demand characterization based on a gravity model is established to quantify the non-uniform spatial distribution of ground communication services. Based on this characterization, three service-aware metrics are designed to evaluate the impact of inter-satellite link failures on end-to-end services.
(3) A hybrid multi-attribute decision-making framework combining the Criteria Importance Through Intercriteria Correlation (CRITIC) method and the entropy weight method is constructed to avoid subjective weighting biases.

The remainder of this paper is organized as follows. Section 2 introduces the system model, including the time-extended graph and traffic demand. Section 3 details the SALC framework. Section 4 presents the simulation results. Section 5 summarizes the paper and outlines future work.

2. Materials and Methods

2.1. LEO Constellations and ISLs

The topology of an LEO satellite constellation is determined by both the constellation configuration and the inter-satellite link connectivity. Most existing LEO satellite constellations adopt the Walker Delta configuration [24], which consists of P orbital planes, each containing S uniformly distributed satellites, so the total number of satellites is $N = P \times S$. For example, the Iridium constellation has $P = 6$ and $S = 11$. The first-generation Starlink constellation comprises five orbital layers and totals 4408 satellites [25,26].

The connectivity of an ISL is determined by the geometric visibility between the two satellites. Let $\mathbf{p}_i(t), \mathbf{p}_j(t) \in \mathbb{R}^3$ be the three-dimensional position vectors of satellite i and j, respectively, at time t. For the link (i, j) to be connected at time t, the distance constraint $\left\|\mathbf{p}_i(t) - \mathbf{p}_j(t)\right\| \leq \mathrm{R}_{\max}$ must be satisfied, and the line connecting the two satellites must not be obstructed by the Earth.

The satellite position vector is derived from the six classical orbital elements (COEs), namely the semi-major axis a, eccentricity e, orbital inclination i, right ascension of the ascending node Ω, argument of perigee ω, and true anomaly v, by solving Kepler's equations and performing a coordinate transformation.

LEO satellite networks rely on ISLs for data relay. Ground users access the space network via gateway stations, and traffic is routed through the ISL mesh to reach the target area. In communication services, end-to-end delay consists of four components: propagation delay, transmission delay, processing delay, and queuing delay. In LEO scenarios, the distance that signals travel in free space is much greater than in terrestrial networks. Since processing delay and queuing delay are influenced by on-board processing

capacity and network congestion, and thus account for only a limited portion of the total delay, propagation delay is the dominant component of end-to-end delay. Propagation delay is determined by the path distance d and the speed of light in a vacuum c_0:

$$D = \frac{d}{c_0}, \tag{1}$$

in this equation, c_0 = 299,792.5 km/s. Since ISL signals propagate through outer space, which is approximately a vacuum, the propagation speed is taken as the speed of light in vacuum. The propagation delay is linearly proportional to the path distance.

It should be noted that additional delay contributions exist in principle, such as relativistic effects and atmospheric effects. For inter-satellite links, signals propagate entirely in outer space and do not pass through the troposphere or ionosphere, so atmospheric delay is negligible. Relativistic effects, including the Shapiro delay and the Sagnac effect, introduce propagation time corrections typically in the picosecond to nanosecond range, which are much smaller than the millisecond-level propagation delay. Therefore, these effects are neglected in this first-level evaluation.

2.2. Temporal Graph Model

Consider a constellation consisting of N LEO satellites, where the set of satellite nodes is denoted as $V = \{1, 2, \ldots, N\}$. Modeling approaches based on static graphs struggle to capture the dynamic evolution of network topology and resources. Therefore, this paper employs temporal graphs to model LEO satellite networks.

Prior to modeling, two basic assumptions are adopted:

Assumption 1. *Each satellite is equipped with a fixed number of ISL transceivers; all ISLs are bidirectional and share a uniform propagation speed.*

Assumption 2. *The connectivity of ISLs is determined solely by geometric visibility between satellites, disregarding external factors such as atmospheric effects and electromagnetic interference.*

Based on the event points at which topology changes occur, the observation time window $[0, T]$ is divided into M discrete time slots. The set of slot indices is denoted as $K = \{1, 2, \ldots, M\}$. The duration of the k-th time slot is Δk, with $\sum_{k=1}^{M} \Delta k = T$. The network topology remains invariant within each time slot, and topology transitions occur only at slot boundaries. Let t_k denote the representative time instant of slot k, defined as the midpoint of the slot, $t_k = t_{k-1} + \Delta k/2$, where the initial time is $t_0 = 0$.

The topological snapshot corresponding to time slot k is an undirected graph $G_k = (V, E_k)$, where $E_k \subseteq V \times V$ is the set of active ISLs within time slot k. The temporal graph of LEO is defined as the sequence of snapshots $G = \{G_1, \ldots, G_M\}$. Figure 1 illustrates an example of such a temporal graph across three consecutive time slots. For each time slot k, a Boolean adjacency matrix $A_k \in \{0, 1\}^{M \times N}$ is defined, where $A_k(i, j) = 1$ if and only if satellites i and j have an ISL in time slot k, and $A_k(i, i) = 0$.

Further, define the distance matrix $D_k \in \mathbb{R}^{N \times N}$, where the matrix element $D_k(i, j) = \left\| \mathbf{p}_i(t) - \mathbf{p}_j(t) \right\|$ represents the propagation distance of the link (i, j) in timeslot k, and $D_k(i, i) = 0$. As can be seen from Equation (1), propagation delay is linearly related to distance. D_k can be directly used as a link weight for path selection and link criticality assessment; the delay values need only be divided by the speed of light, c.

Let $E = \cup_{k=1}^{M} E$ denote the set of all ISLs that occur at least once over the observation window. The temporal graph G represents the temporal evolution of the network topology and provides a dynamic topological basis for evaluating link criticality.

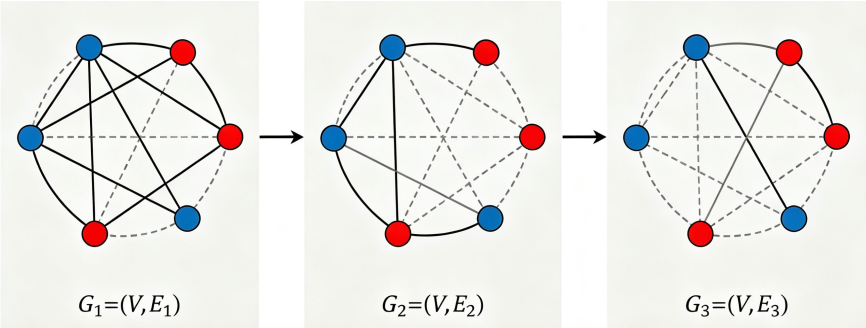


Figure 1. Temporal graph illustration. The network topology evolves over three consecutive time slots. Blue nodes are satellites in the same orbital plane; red nodes are in adjacent planes. Solid lines denote active links; dashed lines indicate links that were active in the previous time slot but are currently disconnected.

2.3. Traffic Demand Model

To quantitatively assess the contribution of ISLs to ground-based services, a mathematical representation of ground-based service demand is required. This section employs the Gravity Model to estimate the distribution of service traffic among cities worldwide and to identify the gateway satellites serving each city.

Consider C core cities as candidate locations for ground gateway stations. The service mass of city c is defined as $D_c = w_c q$, where w_c is the population weight in millions and q_c is the per capita gross domestic product in thousands of U.S. dollars per person, representing the potential communication traffic originating from and destined for that city. Per capita GDP is used here as a simplified proxy for economic demand intensity. It does not directly determine traffic volume, as population, digital penetration, and regional economic structure also matter. This metric has been employed to check if the algorithm works, and other metrics based on other socio-economical factors will be investigated in future.

The Earth is approximated as a sphere with mean radius $R_E = 6371$ km. The longitude and latitude of city c are λ_c and ϕ_c, respectively, and its position vector $\mathbf{g}_c$ in the Earth-Centered Earth-Fixed (ECEF) coordinate system is:

$$\mathbf{g}_c = R_E \begin{bmatrix} \cos\phi_c \cos\lambda_c \\ \cos\phi_c \sin\lambda_c \\ \sin\phi_c \end{bmatrix}, \tag{2}$$

The latitude ϕ_c denotes the geodetic latitude referenced to the WGS84 ellipsoid, consistent with the city coordinate data. For the spherical Earth approximation adopted in this work, the small difference between geodetic and geocentric latitude is neglected. The great-circle distance d_{ij}^{geo} between city i and city j is defined as:

$$d_{ij}^{geo} = R_E \cdot \arccos(\sin\phi_i \sin\phi_j + \cos\phi_i \cos\phi_j \cos(\lambda_j - \lambda_i)), \tag{3}$$

According to the gravity model assumption, the traffic between two cities is proportional to the product of their service masses and inversely proportional to the square of their great-circle distance. The unnormalized traffic volume between city i and city j is given by:

$$\widetilde{T_{ij}} = \frac{D_i D_j}{(d_{ij}^{geo})^2 + \varepsilon}, i \neq j, \tag{4}$$

where $T_{ii} = 0$, and $\varepsilon = 10^{-6}$ is a small perturbation constant to prevent division by zero. Since the squared great-circle distance between distinct cities is typically much larger than ε, the traffic matrix is insensitive to its specific value within a reasonable range, e.g., 10^{-9} to 10^{-3}. The traffic matrix $\mathbf{T} \in \mathbb{R}^{C \times C}$ is then globally normalized as:

$$T_{ij} = \frac{\widetilde{T_{ij}}}{\sum_{m=1}^{C} \sum_{n=1}^{C} \widetilde{T_{mn}}}, \tag{5}$$

where $\sum_{i=1}^{C} \sum_{j=1}^{C} \widetilde{T_{ij}} = 1$.

The midpoint of the observation window is taken as the reference time t_{ref}, and the gateway satellite s_c^* for city c is the satellite geometrically closest to the city's position vector $\mathbf{g}_c$ at that reference time:

$$s_c^* = \underset{s \in V}{\operatorname{argmin}} \left\| \mathbf{p}_s(t_{ref}) - \mathbf{g}_c \right\|, \tag{6}$$

where $\mathbf{p}_s(t_{ref})$ is the three-dimensional position vector of satellite s at time t_{ref}. All traffic from city c is routed through the gateway satellite s_c^* to the space network, and this assignment remains fixed over the entire observation window. The line-of-sight constraint between a ground city and its gateway satellite is implicitly captured by the maximum coverage radius R_{over}, i.e., a satellite can serve a city only if their geometric distance is within R_{over}. The observation window is used solely for temporal topology analysis. Figure 2 illustrates the resulting service demand distribution and gateway assignments.



Figure 2. Service demand distribution and gateway satellite assignment based on the gravity model. City sizes represent service mass, line widths indicate traffic volumes between cities, and star markers denote assigned gateway satellites.

2.4. Problem Formalization

In LEO satellite networks, single ISL failure is a common link-level failure mode, which can be mitigated by rerouting or deploying redundancy. Therefore, identifying the links whose failure most degrades service is of practical importance for link-level protection and recovery. Node criticality cannot directly answer this question, because a node failure removes all incident links simultaneously and measures the joint effect of all incident link failures, rather than the individual effect of each link.

Let $F(G)$ denote the overall service performance of the network under topology G, i.e., the ability of the network to satisfy ground service demands. Node and link criticality are defined as:

$$C_N(v) = F(G) - F(G - \delta(v)), \tag{7}$$

$$C_L(e) = F(G) - F(G - e) \tag{8}$$

where $\delta(v)$ is the set of incident links of node v. $C_N(v)$ is the joint effect of removing all incident links, while $C_L(e)$ is the effect of removing a single link. Because the network performance response to topology changes is nonlinear, node criticality loses the information about the individual contributions of incident links. There is no general function ϕ such that $C_L(e) = \phi(C_N(u), C_N(v))$.

For example, two incident links e_1 and e_2 of node v connect to u_1 and u_2, respectively. If $C_N(u_1) = C_N(u_2)$, but e_1 is the only low-latency relay for a high-traffic city pair and e_2 has equal-delay backup paths, then $C_L(e_1) \neq C_L(e_2)$. Node criticality at both endpoints alone cannot distinguish them. Therefore, link criticality must be evaluated independently.

The central problem addressed in this paper can be formally stated as follows. Given a temporal graph G representing the time-varying topology of an LEO satellite network, and a service demand matrix $\mathbf{T}$ characterizing the non-uniform spatial distribution of ground-based traffic, the objective is to assign a criticality score to each inter-satellite link e that quantifies the degradation of network service capacity resulting from its failure. A higher score indicates a more severe loss when the link fails.

The criticality score is a quantitative measure of the importance of a network element, such as a node or a link, to overall network performance. It is typically derived from centrality, vulnerability, or resilience metrics [27]. In this paper, it is used to rank inter-satellite links according to their impact on service performance.

3. Service-Aware Link Criticality Evaluation Framework

3.1. Framework Overview

Traditional topological centrality methods rely on static network topology characteristics, assuming that all network links carry uniform traffic loads and thereby ignoring regional differences in population density and economic development. Existing service-aware research primarily focuses on evaluating node criticality. Building on this foundation, this paper extends the evaluation granularity to the link level and characterizes the criticality of inter-satellite links from three complementary dimensions: coverage, traffic, and vulnerability. The coverage dimension, denoted as Weighted Coverage Contribution (WCC), quantifies the contribution of an inter-satellite link to ground coverage. The traffic dimension, denoted as Metric of Traffic Awareness (MTA), measures the end-to-end service traffic carried by the link. The vulnerability dimension, denoted as Vulnerability to Path Prolongation (VPP), assesses the increase in end-to-end delay caused by link failure. These three metrics are weighted using a hybrid method that combines the Criteria Importance Through Intercriteria Correlation (CRITIC) method and the entropy weight method, and are then fused via the Technique for Order Preference by Similarity to Ideal Solution (TOPSIS) to generate a comprehensive criticality ranking. Figure 3 illustrates the overall structure of the SALC framework.

3.2. Metric Design

3.2.1. Weighted Coverage Contribution

Coverage capability is a fundamental prerequisite for LEO satellite networks to provide communication services [28]. To characterize the coverage-related importance of an inter-satellite link, we define the Wighted Coverage Contribution (WCC). WCC measures the marginal contribution of the two endpoint satellites of a link to ground coverage. The fewer visible satellites a city has, the greater the coverage contribution of each visible satellite, and thus the more important the associated inter-satellite links are in the coverage dimension.

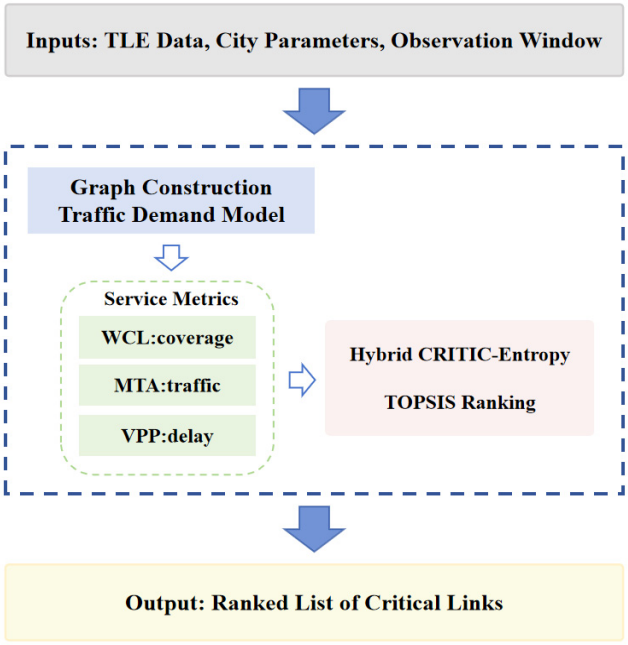


Figure 3. Overall workflow of the SALC evaluation framework. The framework takes TLE data, city parameters, and observation windows as inputs, and proceeds through temporal graph construction, traffic demand modeling, service metric computation, hybrid CRITIC-entropy weighting, and TOPSIS ranking to produce a ranked list of critical links. The blue dashed box denotes the core SALC module, the green dotted box encloses service metrics, and different background colors distinguish functional submodules.

The set of visible satellites for city c in time slot k is defined as

$$S_{k,c} = \{s \in V : \|\mathbf{p_s}(t_k) - \mathbf{g}_c\| \leq R_{\text{cover}}\}, \tag{9}$$

where $\mathbf{p_s}(t_k)$ is the position vector of satellite s at time t_k in time slot k, $\mathbf{g}_c$ is the position vector of city c in the Earth-centered Earth-fixed coordinate system, and R_{cover} is the maximum coverage radius of a satellite.

The WCC for an inter-satellite link $e = (u, v)$ is defined as

$$\text{WCC}(u,v) = \sum_{k=1}^{M}\sum_{c=1}^{C} w_c q_c \cdot \left(\frac{\mathbf{1}\{u \in S_{k,c}\}}{|S_{k,c}| + \varepsilon} + \frac{\mathbf{1}\{v \in S_{k,c}\}}{|S_{k,c}| + \varepsilon}\right), \tag{10}$$

where $\mathbf{1}\{\cdot\}$ is the indicator function, ε is a small constant to prevent division by zero, w_c is the population weight of city c, and q_c is the per capita GDP of city c.

WCC characterizes the marginal contribution of the two endpoint satellites of an inter-satellite link to ground coverage. An inter-satellite link does not directly establish the coverage relationship between a satellite and ground users, but its failure may affect satellite relay and routing, indirectly degrading service coverage. When an endpoint satellite of a link can cover a city, the link contributes to that city's coverage. The denominator introduces the marginal property: the fewer visible satellites a city has, the higher the contribution of each visible satellite. After weighting by $w_c q_c$ and summing over all time slots and cities, WCC measures the overall importance of the link to the coverage of the weighted ground region throughout the observation period.

3.2.2. Multipath Traffic Allocation (MTA)

Multipath routing is widely used in LEO satellite networks to enable parallel traffic transmission and load balancing. The MTA metric measures the weighted service traffic

carried by a given inter-satellite link during end-to-end service transmission [29]. Unlike traditional single-path shortest-path routing, MTA accounts for the fact that, in real-world network scenarios, traffic is distributed across multiple paths due to load balancing, link failures, or dynamic topology changes. The higher the traffic volume carried by a city-pair link, the more significant the impact of a link failure will be, resulting in a higher MTA value.

For city pair (i, j), T_{ij} represents the normalized traffic volume estimated by the gravity model in Section 2. Within time slot k, let $P_k^{(1)} = (i, j)$ denote the shortest-delay path from gateway satellite s_i^* to s_j^*, and $P_k^{(2)} = (i, j)$ denote the second-shortest-delay path; both use the propagation distance $D_k(u, v)$ as the link weight. The MTA for link $e = (u, v)$ is defined as

$$\mathrm{MTA}(u,v) = \sum_{k=1}^{M} \sum_{i=1}^{C} \sum_{j=1}^{C} T_{ij} \cdot [\beta \cdot \mathbf{1}\{(u,v) \in \mathcal{P}_k^{(1)}(i,j)\} + (1-\beta) \cdot \mathbf{1}\{(u,v) \in \mathcal{P}_k^{(2)}(i,j)\}], \tag{11}$$

where $\beta \in [0, 1]$ represents the traffic distribution ratio for the shortest path, reflecting the path diversity in the actual network.

The second path $P_k^{(2)}(i, j)$ is generated as follows. For each edge $e \in P_k^{(1)}(i, j)$, we remove e from the snapshot G_k and compute the shortest-delay path from S_i to S_j in $G_k \setminus \{e\}$. Among these candidates, the path with the minimum delay is selected as $P_k^{(2)}(i, j)$. Therefore, the backup path differs from the primary path by at least one edge, but it is not required to be fully link- or node-disjoint.

The two-path model is adopted because primary/backup routing is common in LEO ISL networks, and the two paths capture the dominant traffic split [30]. Adding more paths would increase computational complexity with diminishing returns for link criticality ranking. The parameter β controls the traffic split and allows the model to represent different degrees of multipath load balancing. We set $\beta = 0.8$, meaning 80% of city-pair traffic is transmitted over the primary path and 20% over the backup path. This setting is consistent with traffic-splitting schemes for LEO satellite networks that favor shorter paths [31]. A sensitivity analysis of β is presented in Section 4.8.

To improve computational efficiency, MTA employs the A* algorithm for pathfinding. Unlike Dijkstra's algorithm, which explores all nodes equally, A* uses a heuristic function to guide the search toward the target, effectively reducing the search space. In LEO satellite networks, the Euclidean distance between satellites in the Earth-centered Earth-fixed coordinate system serves as a reasonable heuristic. For any two satellite nodes a and b, the heuristic function is defined as

$$h(a, b) = \|\mathbf{p}_a(t_k) - \mathbf{p}_b(t_k)\|, \tag{12}$$

3.2.3. Vulnerability Propagation Potential

Time-varying bottleneck links constitute a special class of vulnerable network links whose failure can cause significant deterioration in end-to-end delay [20]. The VPP metric quantifies the delay increase following a link failure to identify such links. When a link fails, the original traffic must be rerouted via alternative paths, resulting in increased end-to-end delay. The greater the delay increment and the higher the traffic volume carried by the corresponding city pair, the more critical the link is to ensuring satellite communication services. VPP measures the degradation in service quality for city pair (i, j) caused by the failure of link e, and it can identify links that, despite carrying limited traffic, serve as critical low-latency pathways.

Let $L_{ij}^{(k)}$ be the shortest-path delay from s_i^* to s_j^* in time slot k, and $L_{ij}^{(k)}(G_k \backslash \{e\})$ be the shortest-path delay after removing link e. The VPP for link $e = (u, v)$ is defined as

$$\mathrm{VPP}(e) = \sum_{k=1}^{M} \sum_{i=1}^{C} \sum_{j=1}^{C} T_{ij} \cdot \max(0, L_{ij}^{(k)}(G_k \backslash \{e\}) - L_{ij}^{(k)}), \tag{13}$$

where T_{ij} is the normalized traffic volume between cities i and j, and $\max(0, \cdot)$ ensures that only the increase in cumulative delay is accounted for. If removing link e results in disconnection between s_i^* and s_j^*, the delay increment for that city pair is assigned a sufficiently large finite constant.

VPP is computed independently for each time slot k. For each snapshot graph G_k, using the propagation distance $D_k(u, v)$ as the edge weight and the Euclidean distance between satellite positions as the heuristic function, an A* search is performed to obtain $L_{ij}^{(k)}$ and $L_{ij}^{(k)}(G_k \backslash \{e\})$.

3.3. Multi-Attribute Decision Fusion

The three service indicators have different units and numerical distribution characteristics. In this section, a hybrid weighting scheme combining the CRITIC method and the entropy weight method is adopted, and the TOPSIS method is used to fuse the three indicators into a unified link criticality score.

3.3.1. Min-Max Normalization

For each link $e \in E$ and each indicator $j \in \{1, 2, 3\}$, corresponding to WCC, MTA, and VPP respectively, the raw score m_{ej} is normalized as

$$x_{ej} = \frac{m_{ej} - m_j^{\min}}{m_j^{\max} - m_j^{\min} + \delta}, \tag{14}$$

where $m_j^{\min} = \min_{e \in E} m_{ej}$, $m_j^{\max} = \max_{e \in E} m_{ej}$, and $\delta = 10^{-6}$ is a small constant to prevent division by zero. The normalized values form a decision matrix $\mathbf{X} \in \mathbb{R}^{|E| \times 3}$, which serves as the input to the hybrid weighting procedure in Section 3.3.2.

3.3.2. Hybrid CRITIC-Entropy Weighting

In this paper, the arithmetic mean of the weights obtained from the entropy weight method and the CRITIC method is used as the composite weight for each indicator.

The entropy weight method assigns weights based on information entropy. Indicators with smaller entropy carry more effective information and receive larger weights [32]. The entropy weight $\omega_j^{Entropy}$ is defined as

$$\omega_j^{Entropy} = \frac{1 - e_j}{\sum_{l=1}^{3} (1 - e_l)}, \sum_{j=1}^{3} \omega_j^{Entropy} = 1, \tag{15}$$

where e_j is the information entropy of indicator j, and l is the summation index over the three indicators.

The CRITIC method determines weights by combining indicator contrast intensity and indicator conflict, measured by the standard deviation and the Pearson correlation coefficients among indicators, respectively [33]. The Pearson correlation coefficient ρ_{jl} measures the conflict between indicators. Highly correlated indicators carry redundant information and receive lower weights, while weakly correlated or negatively correlated indicators provide complementary information and receive higher weights. The Pearson

coefficient is adopted because it is a standard and computationally efficient measure of linear correlation in multi-attribute decision-making.

The CRITIC weight ω_j^{CRITIC} for indicator j is defined as

$$\omega_j^{CRITIC} = \frac{\sigma_j \eta_j}{\sum_{l=1}^{3} \sigma_l \eta_l}, \sum_{j=1}^{3} \omega_j^{CRITIC} = 1, \tag{16}$$

where σ_j is the standard deviation of the normalized values of indicator j, representing its contrast intensity; $\eta_j = \sum_{l=1}^{3} (1 - \rho_{jl})$ is the conflict measure of indicator j, with ρ_{jl} being the Pearson correlation coefficient between indicators j and l, and the summation over l runs over all three indicators.

The hybrid weight is calculated as the arithmetic mean of the entropy weight and the CRITIC weight:

$$\omega_j = \frac{\omega_j^{Entropy} + \omega_j^{CRITIC}}{2}, \sum_{j=1}^{3} \omega_j = 1 \tag{17}$$

This hybrid approach integrates the discriminative power of entropy weighting with the contrast and correlation awareness of CRITIC weighting. The arithmetic mean of the two preserves inter-indicator correlations while capturing data variability, yielding a more balanced and robust weight allocation.

3.3.3. TOPSIS Ranking

The Technique for Order Preference by Similarity to Ideal Solution (TOPSIS) ranks alternatives by calculating their relative proximity to the positive and negative ideal solutions [34].

Construct a weighted normalized decision matrix $Y \in \mathbb{R}^{|E| \times 3}$, where $y_{ej} = \omega_j \cdot x_{ej}$. The positive ideal solution Y^+ and the negative ideal solution Y^- are defined as

$$Y_j^+ = \max_{e \in E} y_{ej}, Y_j^- = \min_{e \in E} y_{ej}, j = 1, 2, 3 \tag{18}$$

the Euclidean distances from link e to the positive and negative ideal solutions are

$$d_e^+ = \sqrt{\sum_{j=1}^{3} (y_{ej} - Y_j^+)^2}, d_e^- = \sqrt{\sum_{j=1}^{3} (y_{ej} - Y_j^-)^2} \tag{19}$$

the comprehensive criticality score for link e is

$$Score(e) = \frac{d_e^-}{d_e^+ + d_e^- + \varepsilon} \tag{20}$$

where ε is a very small constant to prevent division by zero. $Score(e) \in [0, 1]$; a higher score indicates that the link is more critical, performs well across all three service dimensions, and has a greater impact on network service in the event of a failure. The balance and robustness of this hybrid weighting are experimentally validated in Section 4.3.

3.4. Design of a Comprehensive Evaluation Algorithm for Critical Links in Satellite Networks

Based on the three service dimension metrics defined in Section 3.2 and the multi-attribute decision fusion method described in Section 3.3, this section presents the complete workflow of the SALC evaluation algorithm. The workflow consists of five sequential steps, as detailed below.

Temporal graph construction. Construct the temporal graph from TLE-derived satellite positions and geometric visibility.

Traffic matrix calculation. Obtain city-pair traffic via the gravity model and determine the gateway satellite for each city.

Service metric calculation. Compute WCC, MTA, and VPP. Normalize the results to obtain the decision matrix.

Multi-attribute decision fusion. Apply entropy-CRITIC hybrid weighting and TOPSIS to produce the composite criticality score for each link.

Sort all links in descending order of $Score(e)$ and output a ranked list of critical links. Algorithm 1 summarizes the overall computational steps.

Algorithm 1 Service-Aware Link Criticality (SALC) Assessment

Input: TLE data, city set C, time window T, max ISL distance $R_{\max}$
Output: Ranked list of links with criticality scores Score(e)
Construct temporal graph $G = \{G_1, \ldots, G_M\}$ from TLE data
Estimate traffic matrix T via gravity model and assign gateway satellites S_c^*
for each link $(u, v) \in E$ do
    Compute WCC (u, v), MTA(u, v), VPP(u, v)
end for
Normalize three metrics to [0, 1] and get decision matrix X
Compute hybrid weights ω_j
for each link $e \in E$ do
    Compute comprehensive score Score(e) via TOPSIS
end for
Sort all links in descending order of Score(e)
return Link ranking list

The computational complexity of SALC is dominated by the three service metrics: $O(MCN^2)$ for WCC, $O(MC^2N^2 \log N)$ for MTA, and $O(MC^2|E|^2 \log N)$ for VPP, where M is the number of time slots, C is the number of cities, N is the number of satellites, and $|E|$ is the total number of links. The $\log N$ factor arises from the priority queue used in A* search.

To reduce overhead, three strategies are adopted: first, city-pair sampling keeps the top K city pairs based on traffic volumes; second, time-slot sampling selects a uniform subset of slots when M is large; third, parallel computation runs VPP calculations for different links independently across CPU cores.

In practice, since $C \ll N$ and M are typically on the order of tens to hundreds, the algorithm is well suited for offline evaluation of LEO constellations comprising hundreds of satellites.

4. Experimental Analysis

This section presents experimental validation of the proposed SALC evaluation framework. The performance of SALC is assessed through attack experiments, correlation analysis, case studies, and multi-scenario adaptability analysis.

4.1. Experimental Setup

4.1.1. Dataset

The simulation is based on real TLE data from Starlink satellites, sourced from the STARLINK-4 shell. The dataset comprises 668 satellites with an inclination of approximately 53° and an orbital altitude of 530 to 550 km. The observation window is set to 30 min, and an event-driven time-slot partitioning strategy is used to discretize the topology into

61 time slots. The maximum inter-satellite link distance is 2000 km; link connectivity is also subject to line-of-sight constraints. The resulting temporal graph contains 668 satellite nodes and 42,650 inter-satellite links that appear in at least one time slot.

4.1.2. Cities and Traffic Demand

City population and geographic coordinate data were obtained from the GeoNames geographical database [35], and per capita GDP data for each country were sourced from the World Bank's World Development Indicators database [36]. Twelve major global cities were selected as candidate gateway locations: New York, Washington, Seattle, Los Angeles, Frankfurt, London, Paris, Singapore, Tokyo, Hong Kong, Sydney, and São Paulo. Table 1 lists the geographic location, population, per capita GDP, and the resulting service mass for each city. The distribution of service mass is highly skewed, with Tokyo, New York, and London together accounting for 36% of the total. The inter-city traffic matrix was estimated using the gravity model described in Section 2.3.

Table 1. Geographic and service-related parameters of simulated city nodes.

City	Longitude (°)	Latitude (°)	Population (Millions)	GDP per Capita	Service Mass
New York	−74.006	40.713	8.4	85.0	714.0
Washington DC	−77.037	38.907	0.7	90.0	63.0
Seattle	−122.332	47.606	0.7	80.0	56.0
Los Angeles	−118.244	34.052	3.9	75.0	292.5
Frankfurt	8.682	50.111	0.7	70.0	49.0
London	−0.128	51.507	9.0	75.0	675.0
Paris	2.352	48.857	2.2	70.0	154.0
Singapore	103.820	1.352	5.6	80.0	448.0
Tokyo	139.692	35.690	14.0	65.0	910.0
Hong Kong	114.169	22.319	7.5	70.0	525.0
Sydney	151.209	−33.869	5.3	70.0	371.0
Sao Paulo	−46.633	−23.551	12.0	50.0	600.0

Figure 4 shows the geographic distribution of the 12 candidate gateway cities. Figure 5a presents the distribution of communication demand potential across these cities. Figure 5b lists the top 10 city pairs by traffic volume. The top five city pairs, namely London–Paris, Tokyo–Hong Kong, New York–London, Hong Kong–Singapore, and New York–Paris, collectively account for approximately 44.88% of the total traffic, indicating that traffic is highly concentrated along major economic corridors.

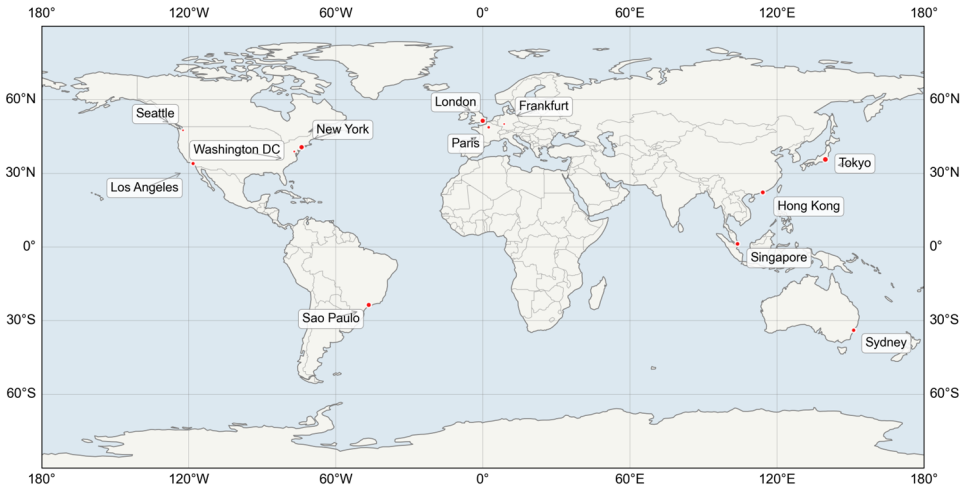
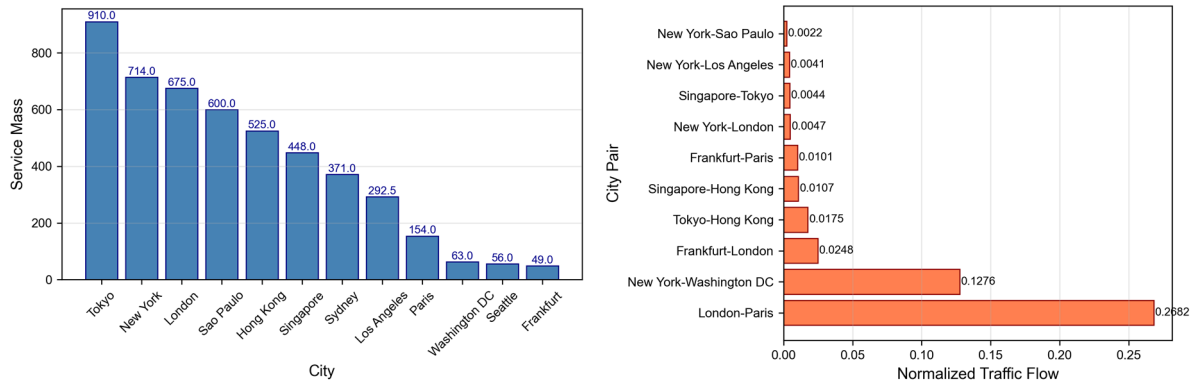


Figure 4. Geographic Distribution of Gateway Cities.



(**a**) (**b**)

Figure 5. Communication Demand and Inter-City Traffic. (**a**) Distribution of service mass for candidate gateway cities; (**b**) Normalized traffic flow of the top 10 city pairs.

4.1.3. Baseline Methods

To evaluate the performance of the proposed SALC framework, we selected the following four baseline methods for comparison.

Service-Aware Temporal Betweenness (SATB). SATB is a service-aware temporal betweenness metric to quantify the importance of satellite nodes for specific end-to-end communication services. We extend this method from node level to link level by counting the number of shortest-delay paths traversing each link, with the link score computed as a traffic-weighted sum of these counts.

Degree Centrality. The degree centrality of a node is the number of its direct neighbors. The link score is taken as the average of the degree centralities of its two endpoints.

Betweenness Centrality. The betweenness centrality of a node measures its frequency of lying on shortest paths. The link score is the average of the betweenness centralities of its two endpoints.

Eigenvector Centrality. The eigenvector centrality of a node considers both its degree and the importance of its neighbors; nodes connected to important nodes receive higher centrality. The link score is the average of the eigenvector centralities of its two endpoints.

Random Sorting. Links are ranked in random order, serving as a lower-bound benchmark.

4.1.4. Sensitivity to Gateway Selection

To justify the fixed-gateway assumption, we compare it with a dynamic-gateway strategy in which each city's gateway satellite is re-selected at every time slot, with all other settings identical. As shown in Table 2, the Spearman rank correlation is 0.99, and the Top-20 Jaccard similarity is 1.00. These results demonstrate that the final SALC ranking and the identified critical link set are highly robust to gateway selection. WCC is independent of gateway selection because it is defined over all visible satellites of each city, rather than the assigned gateway. MTA and VPP may vary locally due to gateway reselection, but these variations are absorbed by the hybrid CRITIC-Entropy weighting and TOPSIS fusion. Although dynamic gateway selection requires per-slot reselection and path recomputation, the fixed midpoint gateway provides a computationally efficient alternative while preserving the final SALC ranking.

Table 2. Sensitivity of the final SALC ranking to gateway selection.

Comparison	Spearman ρ	p-Value	Top-20 Jaccard
Fixed vs. dynamic gateway	0.99	0.01	1.00

4.2. Comparison of Attack Performance

We conduct malicious attack experiments to validate the effectiveness of the SALC evaluation framework. For each link criticality ranking method, we first sort all links in descending order of their scores. Given an attack ratio α, we sequentially remove the first $\alpha \cdot |E|$ links from the top of the ranking, and then recalculate network performance metrics on the compromised temporal graph. The attack ratio α is defined as the fraction of links removed from the criticality ranking, i.e., the number of removed links divided by the total number of links. It ranges from 0 to 1. The set of attack ratios is {0.05,0.10,0.15,0.20,0.30,0.40,0.50}.

The Area Under the Curve (AUC) is defined as the area under the performance decline curve. For a given attack ratio, the faster a method's network performance drops, the smaller its AUC, and the more accurate the identification of critical links.

To evaluate the impact of each method on network performance from multiple perspectives, we introduce four metrics.

Global efficiency measures the overall efficiency of information propagation. Let d_{ij} denote the shortest-path hop count between nodes i and j. Global efficiency E is defined as the average of the reciprocals of all pairwise shortest-path distances:

$$E = \frac{1}{N(N-1)} \sum_{i \neq j} \frac{1}{d_{ij}} \tag{21}$$

A value of E closer to 1 indicates higher propagation efficiency. The decline rate of E during attacks directly reflects the disruption caused by link removals.

Maximum connected component ratio reflects network connectivity integrity after an attack. Let U_k denote the k-th connected component and $|U_k|$ its number of nodes. The ratio L is the size of the largest component normalized by the total number of nodes N:

$$L = \frac{\max_k |U_k|}{N}, \tag{22}$$

A value of L near 1 indicates good connectivity integrity; a decrease in L after link removal implies fragmentation of the network.

Temporal reachability and average temporal distance jointly characterize end-to-end communication capability on a temporal graph. Let $\Re$ be the set of node pairs that are temporally reachable (i.e., satisfying the time-increasing constraint). Temporal reachability R is defined as

$$R = \frac{\Re}{N(N-1)}, \tag{23}$$

The average temporal distance $\overline{D}$ is the mean of the earliest arrival time slots over all reachable pairs, measured in time slots:

$$\overline{D} = \frac{1}{|\Re|} \sum_{(u,v) \in \Re} \tau_s(d) \tag{24}$$

where $\tau_s(d)$ is the earliest arrival time slot from s to d. Higher R and lower $\overline{D}$ indicate better temporal connectivity quality.

As shown in Figure 6, SALC achieves faster network performance degradation under attack. SALC delivers the best performance across all metrics. The AUC for temporal reachability is 1.462, representing reductions of 57.4%, 65.3%, and 69.8% compared to SATB, Eigenvector Centrality, and Random, respectively. The AUC for average temporal distance is 11.375, significantly outperforming all baseline methods. The performance gap between

SALC and the baselines is most pronounced in the early attack stages when $\alpha \leq 0.20$, confirming the framework's effectiveness in identifying critical links. At $\alpha = 0.50$, SALC's reachability drops to 1.34%, while all baseline methods remain above 8.44%.

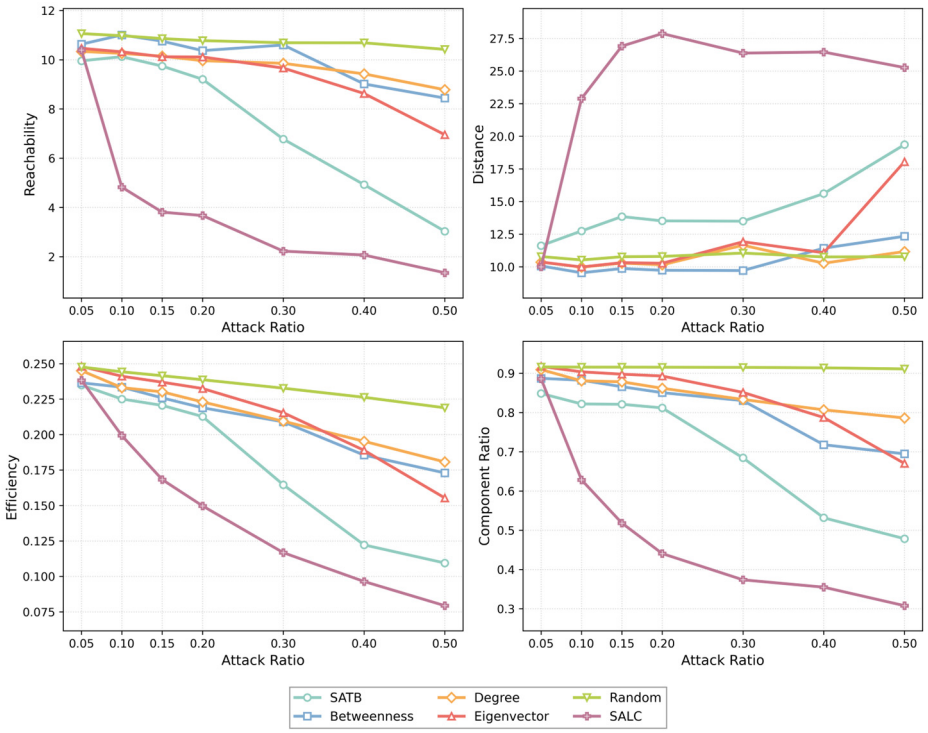


Figure 6. Temporal reachability versus attack ratio for SALC and baseline methods. SALC exhibits the steepest decline in the low attack ratio regime.

Table 3 summarizes the AUC values for all methods in terms of temporal reachability. SALC achieved an AUC of 1.462, significantly outperforming SATB, Degree, Betweenness, Eigenvector Centrality, and Random. Compared to the best baseline, SATB and SALC reduced the AUC by 57.4%. Compared to random sorting, the reduction was 69.8%. These results indicate that the service-aware multi-metric fusion framework is substantially more effective at identifying critical links than traditional topology-centric methods.

Table 3. AUC comparison of different methods across four network performance metrics.

Methods	R	$\overline{D}$	E	L
SALC	1.462	11.375	0.061	0.201
SATB	3.433	6.265	0.081	0.323
Degree	4.393	4.785	0.096	0.379
Betweenness	4.515	4.684	0.093	0.363
Eigenvector	4.219	5.248	0.096	0.377
Random	4.835	4.864	0.105	0.412

4.3. s Weighting Scheme Validation

To validate the hybrid CRITIC–entropy weighting, we benchmark it against equal, entropy-only, and CRITIC-only weighting under identical settings. Table 4 lists the resulting weights and attack AUCs. The hybrid method achieves a balanced weight distribution. By contrast, entropy-only assigns an extremely low weight to WCC, and CRITIC-only assigns an excessively high weight to WCC. The four weighting schemes exhibit comparable attack AUCs, with deviations below 0.5% for temporal reachability and below 0.2% for average

temporal distance. This demonstrates that the hybrid weighting realizes balanced weight assignment while maintaining the attack evaluation performance.

Table 4. Comparison of weighting methods.

Weighting Method	WCC	MTA	VPP	R	$\overline{D}$	E	L
Equal	0.3333	0.3333	0.3333	1.4658	11.3821	0.0608	0.2008
Entropy	0.0560	0.3950	0.5490	1.4589	11.3944	0.0608	0.2008
CRITIC	0.8900	0.0610	0.0490	1.4617	11.3764	0.0608	0.2007
Hybrid	0.4730	0.2280	0.2990	1.4622	11.3750	0.0608	0.2008

To validate the hybrid weighting, Figure 7 compares the balance of the three objective methods using weight entropy and Euclidean distance to the uniform weight vector; higher entropy and smaller distance indicate a more balanced allocation. The hybrid method achieves the highest entropy and the smallest distance. In contrast, entropy-only assigns an extremely low weight to WCC, yielding a large distance, while CRITIC-only assigns an extremely high weight to WCC, yielding the lowest entropy and largest distance. The hybrid method avoids these extremes, still assigning the largest weight to WCC while incorporating MTA and VPP as complementary dimensions, confirming that the hybrid CRITIC–entropy weighting provides a more balanced and robust allocation.

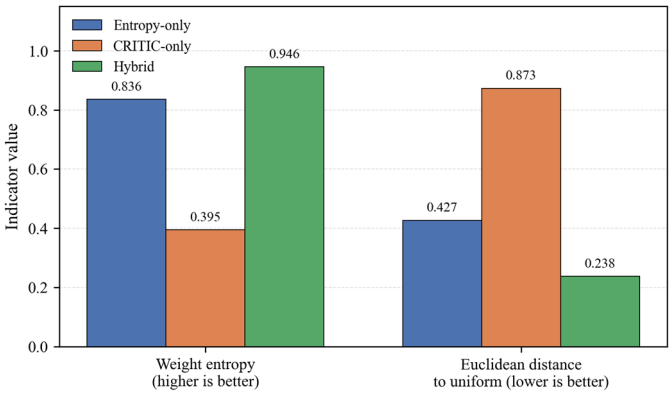


Figure 7. Weight entropy and Euclidean distance to uniform for different weighting methods.

4.4. Ablation Study on Metric Contribution

The Spearman rank correlation coefficient is defined as

$$\rho = 1 - \frac{6\sum_{i=1}^{n} d_i^2}{n(n^2-1)} \tag{25}$$

where d_i is the difference between the ranks of corresponding values and n is the number of samples.

The Spearman correlation matrix among the three normalized metrics is reported in Table 5 WCC is nearly orthogonal to MTA and VPP, indicating that they capture different dimensions of link criticality, while MTA and VPP are moderately correlated.

Table 5. Spearman correlation among the three normalized metrics.

Metrics	WCC	MTA	VPP
WCC	1.000	0.090	0.035
MTA	0.090	1.000	0.466
VPP	0.035	0.466	1.000

The Jaccard similarity coefficient between two sets A and B is defined as

$$J(A, B) = \frac{|A \cap B|}{|A \cup B|}, \tag{26}$$

where $|\cdot|$ denotes the cardinality of a set.

To quantify independent contributions, we count unique links in each metric's Top-K not captured by the other two metrics, and compute pairwise Jaccard overlap. As shown in Table 6, MTA and VPP have 688 and 729 unique links in the Top-1000 (68.8% and 72.9%); Table 7 shows WCC-MTA and WCC-VPP Top-1000 Jaccard are only 0.030 and 0.009, with only 13 links shared by all three metrics. This confirms that MTA and VPP are not redundant but complement WCC in traffic and delay dimensions. Combined with the near-orthogonal correlations, the three metrics provide independent and complementary contributions at the critical-link level.

Table 6. Unique links in the Top-K of each metric.

Top-K	WCC	MTA	VPP
1000	936 (93.6%)	688 (68.8%)	729 (72.9%)
2000	1827 (91.4%)	806 (40.3%)	926 (46.3%)
5000	2989 (59.8%)	620 (12.4%)	750 (15.0%)

Table 7. Pairwise Jaccard overlap of Top-K links.

Metrics	WCC-MTA	WCC-VPP	MTA-VPP
1000	0.030	0.009	0.153
2000	0.044	0.012	0.364
5000	0.250	0.230	0.736

4.5. Correlation Analysis

To understand the relationship between the service-aware SALC scores and the baseline rankings, we calculated the Spearman rank correlation coefficients between SALC and each baseline method.

The results are presented in Table 8, and the corresponding rank scatter plots are shown in Figures 8 and 9. The Spearman correlation coefficient ranges from -1 to 1. The closer its absolute value is to 1, the stronger the agreement between the two rankings; a value close to 0 indicates that the rankings are independent.

Table 8. Spearman correlation between SALC and baselines.

Baseline Methods	Spearman ρ	p
SATB	0.021	1.26×10^{-5}
Degree	-0.467	0.000
Betweenness	-0.385	0.000
Eigenvector	-0.355	0.000
Random	0.001	0.801

The experimental results show a moderate negative correlation between the SALC ranking and traditional topological centrality measures, and these correlations are statistically significant. This confirms that service-aware criticality is not a substitute for topological importance, but rather represents an orthogonal evaluation dimension. SALC and SATB exhibit a correlation close to zero, indicating that node-level service-aware importance and link-level service-aware criticality address fundamentally different problems; node importance cannot be directly mapped to link criticality through a simple

linear relationship. As a control, the correlation coefficient between random sorting and SALC was 0.001 and not statistically significant, which was expected and validates the experimental design.

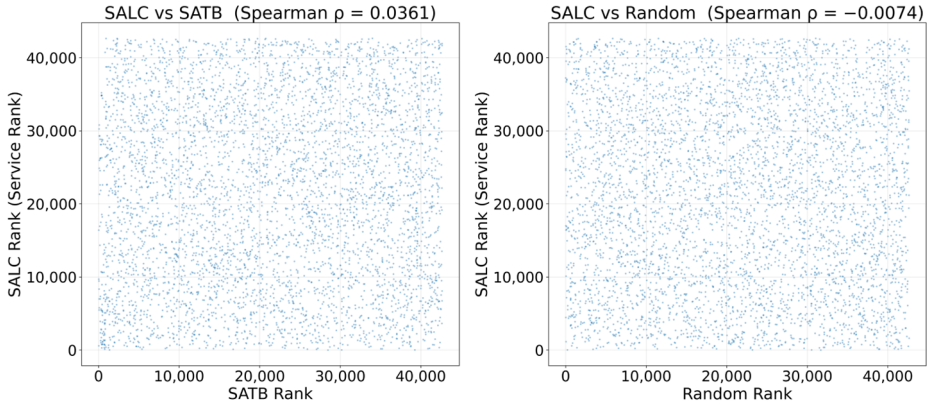


Figure 8. SALC vs. SATB and random rankings.

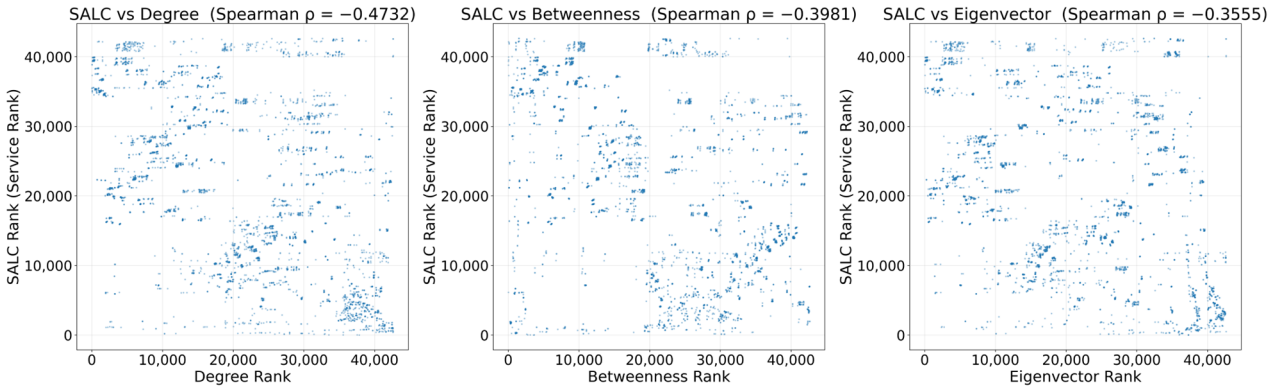


Figure 9. SALC vs. Degree, Betweenness, and Eigenvector rankings.

4.6. Case Study

To compare the SALC framework with topological centrality methods, we conduct a case study to identify links with high service sensitivity but low topological centrality. The topological baseline aggregates time-varying links into a static graph, and scores each link as the average centrality of its two endpoints. We select links with service scores above the 80th percentile and topological scores below the overall median. Figure 10 shows a scatter plot of service versus topological scores, with brighter points denoting the identified links.

Figure 11 shows the temporal connectivity trajectories of the top 5 links throughout the observation window. Among them, link (52, 214) was active in only 1 of the 61 time slots, accounting for just 1.6% of the total, yet it ranked fifth in service criticality. This observation indicates the existence of inter-satellite links that appear sparsely over time but are highly critical from a service perspective. The active time slots for the top-five links accounted for 24.6%, 13.1%, 16.4%, 16.4%, and 1.6% of the total time slots, respectively. During these few active time slots, the links serve as relays for core service traffic. This indicates that SALC can effectively identify inter-satellite links that are active only briefly but are critical to service delivery. Figure 12 visualizes the spatial distribution of these top 5 links, showing that they are geographically dispersed rather than concentrated in a single region.

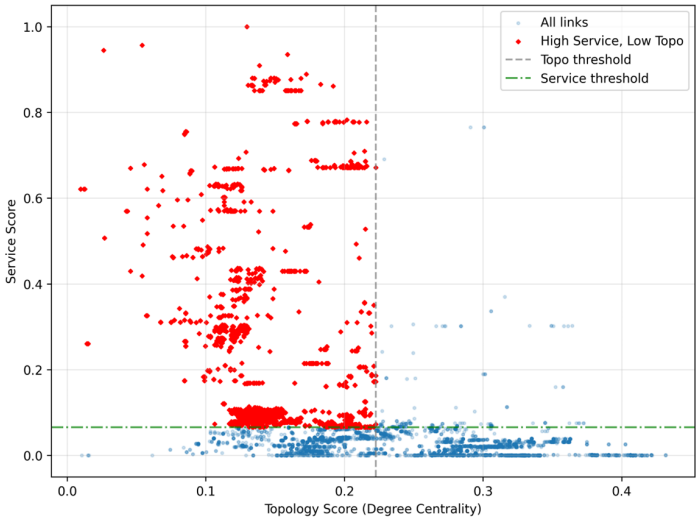


Figure 10. Spearman correlation between SALC scores and baseline rankings.

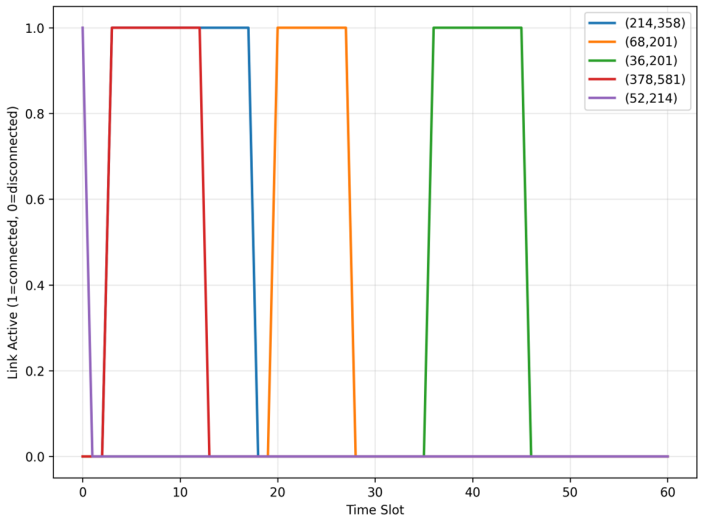


Figure 11. Temporal connectivity of the top-5 links.

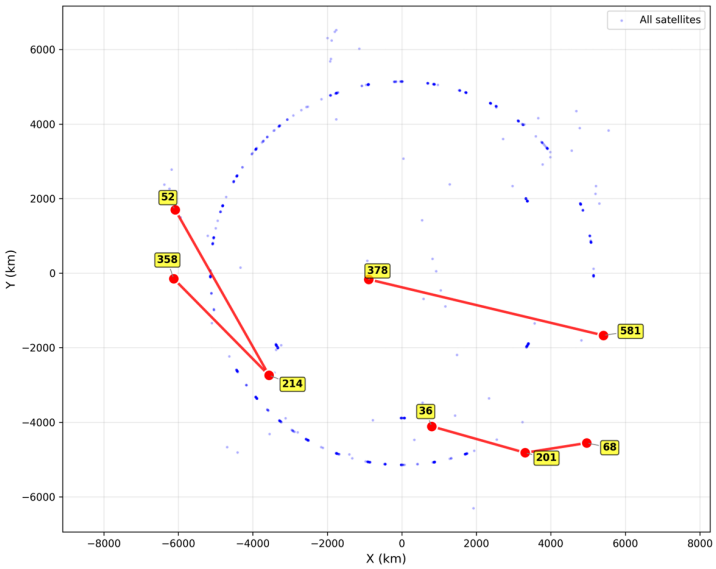


Figure 12. Spatial distribution of the top-5 links. Red circles denote the endpoint satellites of these links, and red lines denote the links.

4.7. Scenario Adaptability Analysis

In this section, four scenarios with different city service weight configurations are designed, as summarized in Table 9.

Table 9. Scenario configurations for adaptability analysis.

Scenario	Traffic Distribution	Focused Cities (Weight = 10)	Purpose
Uniform	Global uniform	None	Baseline
EastAsia	East Asian hotspot	Tokyo, Hong Kong, Singapore	Regional aggregation effect
Hotspot	Trans-Pacific corridor	Previous + New York, Washington DC, Seattle, Los Angeles	Intercontinental traffic effect
Random	Unstructured noise	Random $\in$ [0.1, 10.0]	Noise control

Changes in city weights affect all three metrics simultaneously. WCC responds directly through the satellite-to-ground visibility weighting, while MTA and VPP respond indirectly through the city-pair traffic matrix, reflecting the usage frequency of links in shortest paths and the network-wide delay increment after link failures, respectively. If the three metrics characterize the same underlying physical quantity, scenario changes should not cause drastic fluctuations in the ranking. Conversely, if each metric carries independent information, the set of critical links should shift significantly across scenarios.

Table 10 reports the Jaccard similarity of the top-20 critical links across different scenarios. The Jaccard similarity between the Uniform and EastAsia scenarios is 0.026, indicating that more than 97% of the critical links were re-identified when traffic shifted from a uniform distribution to a single hotspot in East Asia. This dramatic change arises from the differing responses of the three metrics to the same traffic migration. WCC shifts its weighting toward access links over East Asia, while MTA and VPP concentrate their responses on transoceanic backbone links that connect East Asia with other regions. The Jaccard similarity between Uniform and Hotspot is 0.111, further confirming that traffic migration leads to a significant restructuring of the critical link set. The Jaccard coefficients among the three traffic scenarios exhibit a clear gradient: Uniform–EastAsia < Uniform–Hotspot < Hotspot–EastAsia. This order aligns with the actual degree of difference in traffic distribution across scenarios, indicating that the SALC response is continuous and predictable. The Jaccard coefficient between Random and Uniform is 0.667, which is significantly higher than that of any traffic-driven scenario. This suggests that the observed low similarity stems from structural traffic shifts rather than random fluctuations.

Table 10. Jaccard similarity of Top-20 critical links across scenarios.

Scenario	Uniform	Hotspot	EastAsia	Random
Uniform	1.000	0.111	0.026	0.667
Hotspot	0.111	1.000	0.538	0.000
EastAsia	0.026	0.538	1.000	0.000
Random	0.667	0.000	0.000	1.000

Figure 13 illustrates the spatial distribution of the top-20 critical links under different traffic distribution scenarios. Under the uniform scenario, critical links are dispersed globally. When traffic is concentrated in specific regions, critical links become concentrated in those hotspot areas, and inter-satellite links serving hotspot cities are identified as core

links. These results show that SALC can capture the spatial distribution of traffic and dynamically adjust the criticality ranking of links.

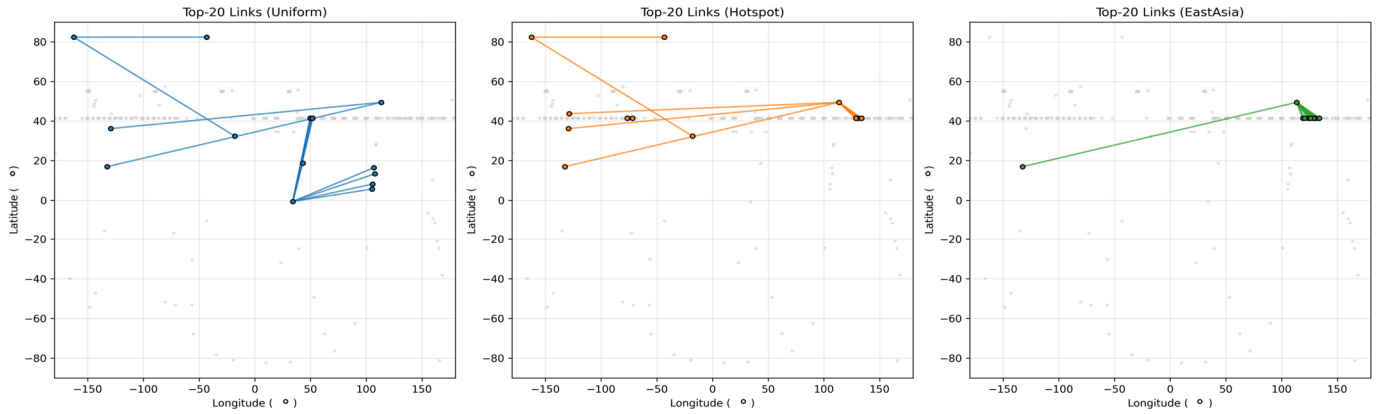


Figure 13. Spatial distribution of the top-20 critical links under different traffic distribution scenarios. Different colors represent different traffic scenarios: blue for Uniform, orange for Hotspot, and green for EastAsia. Circles denote satellite nodes, and lines indicate the top-20 critical links.

4.8. Sensitivity Analysis of the Traffic Split Ratio

The traffic split ratio β in Equation (11) directly affects MTA and the resulting SALC ranking. To verify the choice $\beta = 0.8$, we recomputed the SALC ranking for $\beta \in \{0.0, 0.1, \ldots, 1.0\}$ and analyzed the mean rank shift of links grouped by their baseline rank at $\beta = 0.8$. Figure 14 shows the mean rank shift of the Top-11–50, Top-51–100, and Top-101–500 tiers. The Top-10 links have zero shift for all β, confirming that the most critical links are completely insensitive to β. For the other tiers, the rank shift reaches its minimum at $\beta = 0.8$ and remains within 0.15 positions for $\beta \in [0.6,\ 0.9]$, which we therefore define as the stable interval. Outside this interval, the shift increases sharply: at $\beta = 0.0$ and $\beta = 1.0$, the Top-11–50 shift reaches 22.6 and 47.4, respectively. These results show that β mainly affects medium-criticality links, while the Top-10 critical links remain stable.

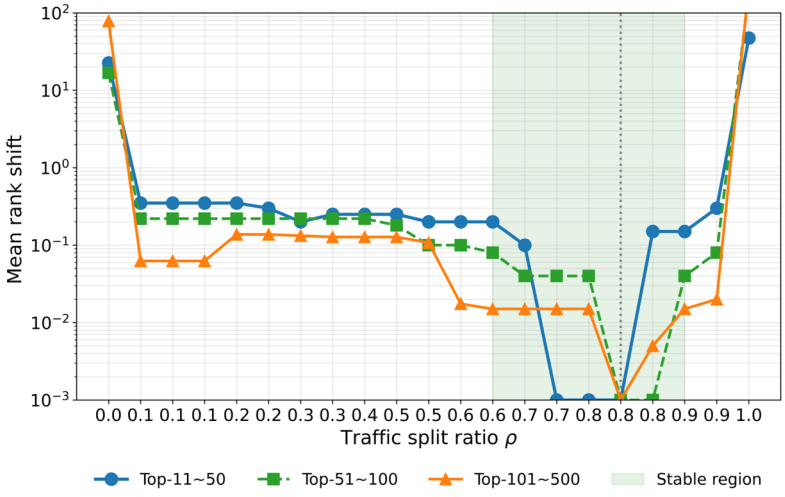


Figure 14. Sensitivity of the SALC ranking to β. The mean rank shift of links in different tiers under rank normalization is used as the metric. Shaded region: stable interval $\beta \in [0.6, 0.9]$.

Since $\beta = 0.8$ lies at the center of the stable interval, we adopt it in our experiments. This choice is also consistent with the principle that the primary path, which provides shorter delay, should carry the majority of traffic.

5. Conclusions

LEO satellite networks are vital for global broadband. However, time-varying topology and non-uniform traffic hinder traditional topology-based methods. This paper proposes an SALC framework. It uses temporal graphs and a gravity model to capture topology dynamics and traffic distribution. Three metrics are designed: WCC, MTA, and VPP. They assess link failures from coverage, traffic, and delay aspects. A hybrid CRITIC-entropy weighting and TOPSIS produce a unified criticality ranking. Experiments on Starlink data show that SALC outperforms baselines and finds critical links missed by topology-based approaches. Future work will use real traffic data and extend to multi-layer satellite networks.

Author Contributions: Conceptualization, X.N. and J.D.; Methodology, X.N. and K.Q.; Software, X.N. and K.Q.; Validation, X.N.; Formal analysis, X.N.; Investigation, X.N.; Resources, X.N. and K.Q.; Data curation, K.Q.; Writing—original draft, X.N.; Writing—review & editing, K.Q. and J.D.; Visualization, X.N.; Supervision, K.Q. and J.D. All authors have read and agreed to the published version of the manuscript.

Funding: This research received no external funding.

Data Availability Statement: The TLE data used in this study are publicly available from CelesTrak (https://celestrak.org, accessed on 11 June 2025). The authors have reviewed and edited the output and take full responsibility for the content of this publication.

Acknowledgments: During the preparation of this manuscript, the authors used DeepSeek-V4.1 Flash for translation purposes. The authors have reviewed and edited the output and take full responsibility for the content of this publication. We also thank Liu for her substantial contributions during the major revision, including mathematical corrections, complexity analysis, sensitivity analysis, ablation study, figure improvements, and preparation of reviewer responses. She has consented to be acknowledged here.

Conflicts of Interest: The authors declare no conflict of interest.

Abbreviations

The following abbreviations are used in this manuscript:

LEO	Low Earth Orbit
ISL	Inter-Satellite Link
GEO	Geostationary Earth Orbit
SATB	Service-Aware Temporal Betweenness
TLE	Two-Line Element
ECEF	Earth-Centered Earth-Fixed
WCC	Weighted Coverage Contribution
MTA	Multipath Traffic Allocation
VPP	Vulnerability Propagation Potential
CRITIC	Criteria Importance Through Intercriteria Correlation
TOPSIS	Technique for Order Preference by Similarity to Ideal Solution
SALC	Service-Aware Link Criticality

References

1. He, W.; Li, H.; Qiu, S. GNN-ASSSP: A Study of an Attention Mechanism Driven Dynamic Routing Algorithm for LEO Satellite Networks. *Aerosp. Sci. Technol.* **2025**, *178*, 112361. [CrossRef]
2. Kang, S.-Y.; Jo, M.-S.; Choi, J.-Y.; Yang, S.S. Cost Effectiveness of Reusable Launch Vehicles Depending on the Payload Capacity. *Aerospace* **2025**, *12*, 364. [CrossRef]
3. Zhang, H.; Wang, Z.; Zhang, S.; Meng, Q.; Luo, H. Link-Identified Routing Architecture in Space. *IEEE Trans. Netw. Sci. Eng.* **2025**, *12*, 392–408. [CrossRef]

4. Liu, H.; Guan, X.; Wan, X.; Yang, F. All-Time Dynamic Minimum Spanning Tree for Inter-Satellite Link Optimization in LEO Networks. *IEEE Trans. Netw. Serv. Manag.* **2025**, *22*, 4577–4589. [CrossRef]
5. Chen, Q.; Yang, L.; Zhao, Y.; Wang, Y.; Zhou, H.; Chen, X. 3-ISL Topology: Routing Properties and Performance in LEO Megaconstellation Networks. *IEEE Trans. Aerosp. Electron. Syst.* **2025**, *61*, 4961–4972. [CrossRef]
6. Zhou, E.; Kobayashi, M.; Fujihashi, T.; Alim, M.A.; Saruwatari, S.; Nishi, M.; Watanabe, T. Dynamic Cluster Multicast Routing for Walker Delta LEO Satellite Mega-Constellations. *IEEE Trans. Aerosp. Electron. Syst.* **2026**, *62*, 1609–1629. [CrossRef]
7. Zhang, L.; Du, Y.; Zhang, Y.; Tang, Y. Distributed Anti-Cascading Routing Scheme Based on Fuzzy Logic in LEO Satellite Networks. *IEEE Trans. Veh. Technol.* **2025**, *74*, 3196–3211. [CrossRef]
8. Du, J.; Zhang, R.; Hu, J.; Xia, T.; Liu, J. Fast Reroute Mechanism for Satellite Networks Based on Segment Routing and Dual Timers Switching. *Aerospace* **2025**, *12*, 233. [CrossRef]
9. Tian, Q.; Yang, P.; Zhang, J.; Chen, R. Improved Importance Contribution Method for Node Importance Evaluation in Space Information Network. In Proceedings of the 2023 6th International Conference on Artificial Intelligence and Big Data (ICAIBD 2023), Chengdu, China, 26–29 May 2023; pp. 609–617.
10. Zhou, R.; Zhang, Q.; Tao, Y.; Shen, Y.; Zhang, W.; Tian, F.; Tian, Q.; Qian, J. Intelligent Multipath Backup Ant Colony Routing Algorithm of Satellite Network Based on Betweenness Centrality. In Proceedings of the 2020 IEEE Computing, Communications and IoT Applications (ComComAp 2020), Beijing, China, 20–22 December 2020.
11. Gao, Q.; Hu, M.; Yang, L.; Zhao, Z. Identification of Key Nodes in Multi-Layer Heterogeneous Aviation Network through Aggregating Multi-Source Information. *Aerospace* **2024**, *11*, 619. [CrossRef]
12. Xu, R.; Di, X.; He, X.; Qi, H. Evaluation Method of Node Importance in Temporal Satellite Networks Based on Time Slot Correlation. *EURASIP J. Wirel. Commun. Netw.* **2021**, *2021*, 188. [CrossRef]
13. Wang, S.; Zhao, Y.; Xie, H. PKN: Improving Survivability of LEO Satellite Network through Protecting Key Nodes. In *Proceedings of the 15th International Conference on Emerging Networking EXperiments and Technologies*; Association for Computing Machinery: New York, NY, USA, 9–12 December 2019; pp. 7–8.
14. Zou, Y.-W.; Deng, H.-T.; Ye, Z.-C.; Sun, S.-M.; Zhang, T.; Luo, Z.-F. Identifying Key Nodes of Mega LEO Satellite Network Based on Node Embedding and Machine Learning. In Proceedings of the International Astronautical Congress (IAC), Baku, Azerbaijan, 2–6 October 2023; Volume 2023.
15. Tianming, Z.; Jie, Z.; Cibo, Y.U.; Lu, C.; Yunjun, G.A.O.; Bin, C.A.O.; Jing, F.A.N.; Ge, Y.U. Labeling-Based Centrality Approaches for Identifying Critical Edges on Temporal Graphs. *Front. Comput. Sci.* **2025**, *19*, 192601. [CrossRef]
16. Pan, R.K.; Saramaki, J. Path Lengths, Correlations, and Centrality in Temporal Networks. *Phys. Rev. E Stat. Nonlinear Soft Matter Phys.* **2011**, *84*, 016105. [CrossRef] [PubMed]
17. Buc, S.; Molter, H.; Niedermeier, R.; Rymar, M. Algorithmic Aspects of Temporal Betweenness. In Proceedings of the ACM SIGKDD International Conference on Knowledge Discovery and Data Mining, San Diego, CA, USA, 6–10 July 2020; pp. 2084–2092.
18. Zhang, Z.; Jiang, C.; Guo, S.; Qian, Y.; Ren, Y. Temporal Centrality-Balanced Traffic Management for Space Satellite Networks. *IEEE Trans. Veh. Technol.* **2018**, *67*, 4427–4439. [CrossRef]
19. Bi, Y.; Liu, R.; Sheng, M.; Li, J.; Wu, W.; Wu, J.; Wang, Z. Exploring on the Critical Link Sequence of Satellite Networks. In Proceedings of the 2019 IEEE 89th Vehicular Technology Conference (VTC2019-Spring), Kuala Lumpur, Malaysia, 28 April–1 May 2019; pp. 1–6.
20. Deng, Y.; Wu, Q.; Lai, Z.; Gu, C.; Li, H.; Li, Y.; Liu, J. Time-Varying Bottleneck Links in LEO Satellite Networks: Identification, Exploits, and Countermeasures. In Proceedings of the 2025 Network and Distributed System Security Symposium, San Diego, CA, USA, 24–28 February 2025.
21. Guo, B.; Xiong, Z.; Zhang, Z.; Li, B.; Niyato, D.; Yuen, C.; Han, Z. Resilience of Mega-Satellite Constellations: How Node Failures Impact Inter-Satellite Networking Over Time? *IEEE Trans. Commun.* **2025**, *73*, 15705–15721. [CrossRef]
22. Gong, S.; Tang, L.; Wang, J.; Chen, Q.; Zhu, C. *A Key Node Set Analysis Method for Regional Service Denial in Mega-Constellation Networks*; IEEE: New York, NY, USA, 2025.
23. Liu, Y.; Yang, Y.; Wang, T. CosmoBalancer: A Service-Aware Load Balancing System for High-Performance Satellite Service Clusters. In Proceedings of the 9th Asia-Pacific Workshop on Networking (APNet 2025), Shanghai, China, 7–8 August 2025; pp. 263–264.
24. Zhang, D.; Xu, Z.; Zhu, Y.; Cheng, H.; Yuan, X.; Jin, Z. A Unified Analytical Framework for ISL Visibility Modeling, Antenna Pointing, and Residual Time Estimation in LEO Constellations. *Aerosp. Sci. Technol.* **2026**, *178*, 113147. [CrossRef]
25. Anderson, B.J.; Angappan, R.; Barik, A.; Vines, S.K.; Stanley, S.; Bernasconi, P.N.; Korth, H.; Barnes, R.J. Iridium Communications Satellite Constellation Data for Study of Earth's Magnetic Field. *Geochem. Geophys. Geosys.* **2021**, *22*, e2020GC009515. [CrossRef]
26. Lu, W.; Wang, Z.; Zhang, H.; Zhang, S.; Luo, H. OpenSN: An Open Source Library for Emulating LEO Satellite Networks. *IEEE Trans. Parallel Distrib. Syst.* **2025**, *36*, 1574–1590. [CrossRef]
27. Kurmankhojayev, D.; Li, G.; Chen, A. Link Criticality Index: Refinement, Framework Extension, and a Case Study. *Reliab. Eng. Syst. Saf.* **2024**, *243*, 109889. [CrossRef]

28. del Portillo, I.; Cameron, B.G.; Crawley, E.F. A Technical Comparison of Three Low Earth Orbit Satellite Constellation Systems to Provide Global Broadband. *Acta Astronaut.* **2019**, *159*, 123–135. [CrossRef]
29. Huang, Y.; Yang, D.; Feng, B.; Tian, A.; Dong, P.; Yu, S.; Zhang, H. A GNN-Enabled Multipath Routing Algorithm for Spatial-Temporal Varying LEO Satellite Networks. *IEEE Trans. Veh. Technol.* **2024**, *73*, 5454–5468. [CrossRef]
30. Brady, C.; Sun, J.; Yuksel, M.; Shake, T. PRABR: Integrating Primary and Backup Routing in pLEO Satellite Networks. In Proceedings of the IEEE Aerospace Conference, Big Sky, MT, USA, 1–8 March 2025.
31. Zhang, S.; Li, X.; Yeung, K.L. Segment Routing for Traffic Engineering and Effective Recovery in Low-Earth Orbit Satellite Constellations. *Digit. Commun. Netw.* **2024**, *10*, 706–715. [CrossRef]
32. Zhou, J.; Zhu, X.; Yao, H. Resilience Evaluation and Optimization Method of Large-Scale LEO Satellite Networks Based on Entropy Theory. *IEEE Internet Things J.* **2025**, *12*, 37940–37961. [CrossRef]
33. Ashja-Ardalan, S.; Alesheikh, A.A.; Sharif, M.; Wittowsky, D. Resilience of Urban Road Networks to Climate Change: A Spatial-Topological Approach. *Transp. Res. Part D Transp. Environ.* **2025**, *148*, 104948. [CrossRef]
34. Amozegay, F.; Kosari, A.; Labibian, A. Inter-Satellite Link Optimization of Two Collocated Geostationary Satellites. *IEEE Access* **2025**, *13*, 206825–206843. [CrossRef]
35. GeoNames. GeoNames Geographical Database. Available online: https://www.geonames.org (accessed on 1 October 2025).
36. The World Bank. World Development Indicators. Available online: https://databank.worldbank.org/source/world-development-indicators (accessed on 1 October 2025).

Disclaimer/Publisher's Note: The statements, opinions and data contained in all publications are solely those of the individual author(s) and contributor(s) and not of MDPI and/or the editor(s). MDPI and/or the editor(s) disclaim responsibility for any injury to people or property resulting from any ideas, methods, instructions or products referred to in the content.